nature structural & molecular biology

Substrate protein folds while it is bound to the ATP-independent chaperone Spy

Frederick Stull[1,3], Philipp Koldewey[1,3], Julia R Humes[2], Sheena E Radford[2] & James C A Bardwell[1]

Chaperones assist in the folding of many proteins in the cell. Although the most well-studied chaperones use cycles of ATP binding and hydrolysis to assist in protein folding, a number of chaperones have been identified that promote folding in the absence of high-energy cofactors. Precisely how ATP-independent chaperones accomplish this feat is unclear. Here we characterized the kinetic mechanism of substrate folding by the small ATP-independent chaperone Spy from *Escherichia coli*. Spy rapidly associates with its substrate, immunity protein 7 (Im7), thereby eliminating Im7's potential for aggregation. Remarkably, Spy then allows Im7 to fully fold into its native state while it remains bound to the surface of the chaperone. These results establish a potentially widespread mechanism whereby ATP-independent chaperones assist in protein refolding. They also provide compelling evidence that substrate proteins can fold while being continuously bound to a chaperone.

Chaperones are essential for maintaining protein-folding homeostasis, and they have important roles in the cellular stress response. By binding to aggregation-sensitive folding intermediates, chaperones inhibit aberrant interactions between proteins. The most intensively studied folding chaperones, such as the GroEL–GroES and DnaK systems, facilitate substrate protein folding through ATP- and cofactor-driven conformational changes[1–5]. These conformational changes convert ATP-dependent folding chaperones from a state with a high affinity for substrates to a state with a low affinity for substrates, thereby allowing substrate proteins to be released. It is widely thought that this change in affinity is needed to release bound substrates into bulk solution or, in the case of GroEL–GroES, into the unbound interior of the chaperonin cavity, where folding of the substrate protein occurs[1,3–6].

In contrast to ATP-dependent chaperones, a number of chaperones have been identified that can assist in protein folding in the absence of ATP[7–11]. The mechanism by which ATP-independent chaperones promote substrate protein folding without a means of regulating substrate binding and release is not clear. One recently discovered ATP-independent chaperone is Spy, which was identified through a genetic selection to enhance *in vivo* protein stability in *Escherichia coli*[10]. Spy is a cradle-shaped, dimeric α-helical protein that is massively and rapidly upregulated upon exposure to protein-folding stresses such as exposure to butanol or tannins[10,12,13]. Spy increases from a near-zero level under nonstress conditions to a level representing 20–50% of the periplasmic proteome during stress[10,12,13]. This major investment of cellular resources in the production of Spy under stress conditions implies that there is a pressing need for Spy *in vivo* during stress. *In vitro* experiments have revealed that Spy both inhibits the aggregation of proteins and enhances the refolding yield of proteins in an ATP-independent manner[10,14].

The mechanism by which Spy and the growing class of ATP-independent chaperones function to refold proteins in the absence of energy cofactors is an unresolved question. We addressed this by determining how Spy affects the folding pathway of Im7, the protein that was used to discover Spy. Im7 has a number of attributes that facilitate its study. It is small and monomeric, and it folds via a well-characterized mechanism that involves transition through a partially folded on-pathway intermediate before the native state is reached[15–20]. The fluorescence of the lone tryptophan residue in Im7 is a sensitive reporter of the folding status of the substrate: the unfolded state of Im7 ($Im7_U$) is moderately fluorescent, the partially folded intermediate state ($Im7_I$) is hyperfluorescent, and the native state ($Im7_N$) is weakly fluorescent[16,20]. In addition, variants of Im7 have been developed that mimic $Im7_U$ (Im7 L18A L19A L37A) or $Im7_I$ (Im7 L53A I54A). Under neutral pH, the $Im7_U$ mimic is unfolded, and the $Im7_I$ mimic closely resembles the hyperfluorescent intermediate state[21–24]. The small size and biochemical accessibility of Spy-Im7 provide a powerful system (diagramed in **Fig. 1**) to address the open question of exactly how ATP-independent chaperones affect the folding of proteins. In particular, we decided to address whether proteins can fold while they are bound to a chaperone, or whether they instead are arrested at a defined state in the folding energy landscape and rely upon release for continued folding. We set out to analyze the ability of Spy to bind to three low-energy states that compose the Im7 folding pathway, as well as the effect of Spy on the kinetic mechanism of Im7 folding (**Fig. 1**). We show here that Spy binds the unfolded, intermediate and native states of Im7 with comparable (micromolar) affinities, thus allowing Im7 to fold completely into the native state while it is bound to the chaperone. By doing so, Spy minimizes the concentration of unbound unfolded or partially folded proteins,

[1]Howard Hughes Medical Institute, Department of Molecular, Cellular and Developmental Biology, University of Michigan, Ann Arbor, Michigan, USA. [2]Astbury Centre for Structural and Molecular Biology, School of Molecular and Cellular Biology, University of Leeds, Leeds, UK. [3]These authors contributed equally to this work. Correspondence should be addressed to F.S. (fstull@umich.edu), S.E.R. (s.e.radford@leeds.ac.uk) or J.C.A.B. (jbardwel@umich.edu).

Received 17 August; accepted 2 November; published online 30 November 2015; doi:10.1038/nsmb.3133

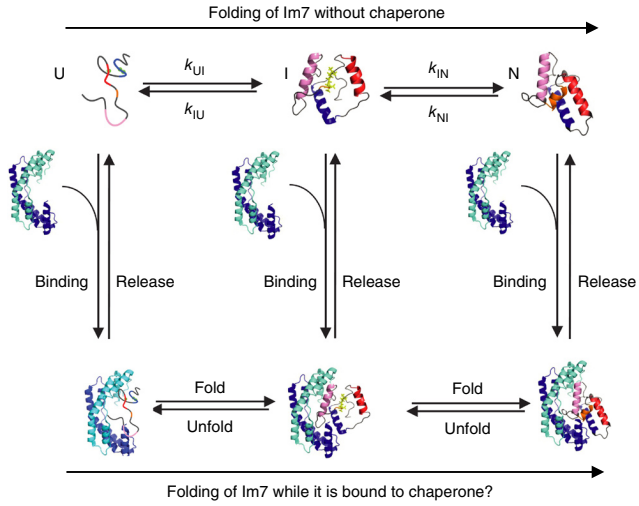

Figure 1 Folding of the protein Im7 in the presence or absence of the chaperone Spy. Im7 is shown as a multicolored protein that is helical in both the folding intermediate (I) and in the native folded state (N) and lacks any persistent secondary structure in the unfolded state (U). Spy is shown as a blue cradle-shaped homodimer. Spy binding and release are shown as vertical arrows.

thus suppressing their tendency to aggregate. Once the folding stress is removed, Spy is presumably diluted by degradation or cell growth, thereby releasing bound substrate without the need for energy provided by ATP binding and/or hydrolysis.

RESULTS

Spy binds the three states on the Im7 folding energy landscape

We first investigated whether Spy is able to interact with three low-energy states that compose the Im7 folding pathway (**Fig. 1**). We did this by using isothermal titration calorimetry (ITC) to monitor binding of Spy to Im7 L18A L19A L37A ($Im7_U$ mimic), Im7 L53A I54A ($Im7_I$ mimic) and native wild-type (WT) Im7 and found that Spy binds to all three variants of Im7, with affinities of 10.4 μM, 3.5 μM and 20.5 μM, respectively (**Fig. 2**). In all cases, we observed a stoichiometry of one Spy dimer per Im7. Therefore, Spy binds all three populated states on the Im7 folding energy landscape with comparable affinities.

Spy rapidly binds unfolded Im7

We decided to further examine Spy-Im7 binding and, more importantly, how the binding reaction might alter the distribution of Im7 between the different states on the folding energy landscape (**Fig. 1**). To do this, we first measured the kinetics of the interaction between Spy and the $Im7_U$ mimic, the $Im7_I$ mimic or Im7 WT by stopped-flow fluorescence, using the tryptophan of Im7 as a reporter. Because Spy lacks tryptophan residues, the signal change reflects the environment of the lone tryptophan (W75) in Im7 and hence reports on the folding state of the protein substrate.

Upon binding of Spy to the constitutively unfolded $Im7_U$ mimic, the tryptophan fluorescence intensity rapidly increased (**Fig. 3a**). The observed rate constant (k_{obs}) of the association reaction increased linearly with Spy concentration (**Fig. 3a**), in agreement with a bimolecular reaction in which Spy binds directly to $Im7_U$. Fitting the plot of k_{obs} against Spy concentration to a straight line yielded a bimolecular association rate constant (k_{on}) of $1.3 \pm 0.2 \times 10^7$ M^{-1} s^{-1} and a dissociation rate constant (k_{off}) of 210 ± 20 s^{-1} (mean ± s.e.m. of fit). Under butanol or tannin stress, the concentration of Spy is ~2 mM *in vivo*[10,12,13]. At this concentration, association between Spy and $Im7_U$ would be very rapid (occurring with a half-time of 26 μs).

An important *in vivo* consequence of the rapid association between Spy and $Im7_U$ is that under stress conditions, Im7 (and presumably other unfolded aggregation-prone proteins) would have very little time to aggregate before being bound by Spy.

Binding to Spy alters the conformation of the Im7 intermediate

In contrast to the fluorescence increase that occurred upon binding of Spy to the $Im7_U$ mimic, the addition of Spy to the $Im7_I$ mimic caused a fluorescence decrease (**Fig. 3b**). This change could reflect quenching of the fluorescence of W75 in the Spy–$Im7_I$ mimic complex or a conformational change in the $Im7_I$ mimic that occurs after binding to Spy.

These two possibilities can be distinguished by measuring the dependence of k_{obs} of the fluorescence change on Spy concentration. If the change in fluorescence were to occur upon Spy binding, k_{obs} should increase linearly with Spy concentration, in agreement with a bimolecular reaction. Instead, we observed that k_{obs} increased hyperbolically with Spy concentration (**Fig. 3b**), in agreement with a two-step mechanism wherein Spy first binds the $Im7_I$ mimic, and then a conformational change occurs within the complex[25,26]. Extrapolation of the traces back to time zero showed that the initial fluorescence of the binding reaction was identical to the fluorescence of the $Im7_I$ mimic alone (**Supplementary Fig. 1**); i.e., the fluorescence of the $Im7_I$ mimic alone was equal to the fluorescence of the Spy–$Im7_I$ mimic complex before the conformational change. Thus, it appears that the initial bimolecular step in which Spy binds the $Im7_I$ mimic is not detectable by fluorescence. Instead, it is the subsequent conformational change within the complex that can be observed through

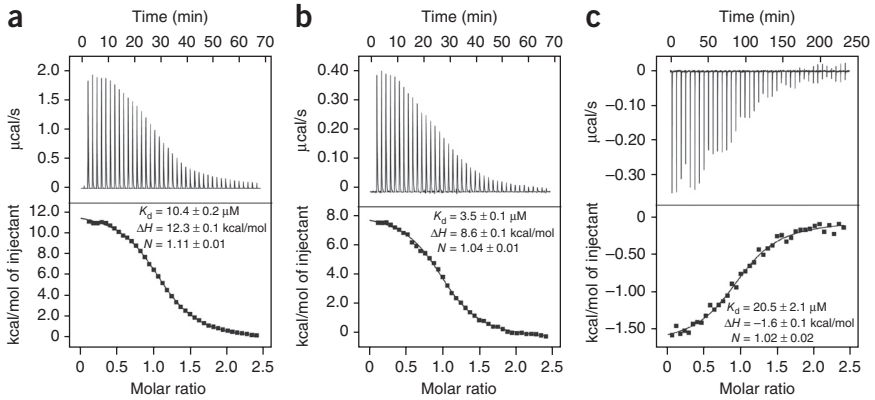

Figure 2 ITC titrations for Spy binding to Im7 WT and variants. (**a**) Titration of 150 μM Im7 L18A L19A L37A ($Im7_U$ mimic) in the cell with 1.65 mM Spy dimer in the syringe. (**b**) Titration of 50 μM Im7 L53A I54A ($Im7_I$ mimic) in the cell with 550 μM Spy dimer in the syringe. (**c**) Titration of 230 μM Im7 WT in the cell with 2.53 mM Spy dimer in the syringe. All titrations were performed in 40 mM HEPES-KOH, pH 7.5, and 100 mM NaCl at 10 °C. The black lines in the bottom panels are the best fit of the data to a one-site model. Values reported are the mean ± s.e.m. of the fit. ΔH, enthalpy; N, stoichiometry of binding.

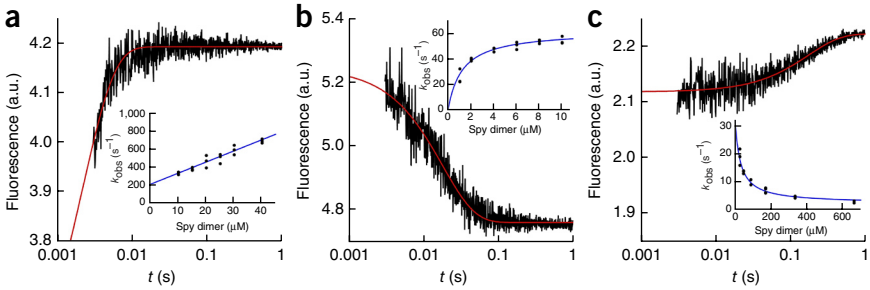

Figure 3 Kinetics of Spy binding to $Im7_U$, $Im7_I$ and $Im7_N$. (**a**–**c**) Graphs showing the change in tryptophan fluorescence associated with Spy binding to 1 μM $Im7_U$ mimic (**a**), 0.5 μM $Im7_I$ mimic (**b**) and 4.8 μM Im7 WT (**c**) on a logarithmic timescale. *t*, time; a.u., arbitrary units. The red lines are the best fit of each data set to a single exponential. The insets show the change in observed rate constant with Spy concentration for each variant of Im7. Each data point in the insets represents the average of 10–15 traces. For Spy binding to $Im7_U$ mimic, k_{obs} increased linearly with Spy concentration, thus indicating that Spy can bind $Im7_U$, and yielding a k_{on} of $1.3 \pm 0.1 \times 10^7$ M^{-1} s^{-1} and a k_{off} of 210 ± 20 s^{-1}. For Spy binding to the $Im7_I$ mimic, k_{obs} increased hyperbolically with Spy concentration, reaching a limiting value of 62 ± 2 s^{-1}, which is consistent with Spy binding to $Im7_I$ being followed by partial folding or unfolding of Im7 within the complex. For Spy binding to Im7 WT, k_{obs} decreased with Spy concentration, reaching a limiting value of 3.3 ± 0.9 s^{-1}. Values reported are the mean ± s.e.m. of the fit. In combination with the burst phase when Spy binds Im7 WT (**Fig. 4a**), this decreasing k_{obs} suggests that Spy can bind $Im7_N$, which then partially unfolds to $Im7_I$ while it is bound.

fluorescence. Because $Im7_I$ is hyperfluorescent relative to both $Im7_U$ and $Im7_N$, the fluorescence decrease associated with this conformational change would be consistent with either unfolding of the intermediate or folding to the native state while Im7 is bound to Spy. Thus, $Im7_I$ can either fold or unfold while it is bound to Spy.

Spy binds to native Im7 and unfolds it while it is bound

The conformational change that occurs in the $Im7_I$ mimic while it is bound to Spy led us to explore the possibility that a conformational change might also occur in $Im7_N$ upon binding to Spy. Again using stopped-flow fluorescence, we found that the fluorescence intensity of Im7 WT increased upon binding to Spy (**Fig. 3c**). The initial fluorescence intensities observed in the dead time (3.5 ms) of Spy binding to Im7 WT were higher than the fluorescence of Im7 WT alone (fluorescence of 1.78 arbitrary units in **Fig. 4a**), thus indicating that at least one step occurred within the dead time of the instrument (**Fig. 4a**). This burst in fluorescence reached a saturating value at high Spy concentrations, a result probably reflecting the rapid binding of Spy to $Im7_N$, which caused an increase in the tryptophan fluorescence of $Im7_N$ (**Supplementary Fig. 2a**). This rapid binding was followed by a small, slow exponential increase in fluorescence. The k_{obs} for the slower postburst-phase step decreased hyperbolically with Spy concentration, asymptotically reaching a limiting value (~3 s^{-1}) (**Fig. 3c**). The hyperbolically decreasing k_{obs} is consistent with the postburst-phase step monitoring a change in the equilibrium constant between $Im7_N$ and another conformation of Im7 that is more fluorescent than $Im7_N$ and is caused by Spy binding[25,26]. This conformation is probably $Im7_I$, because $Im7_I$ is hyperfluorescent relative to $Im7_N$. The magnitude of the fluorescence increase that occurs after Spy–Im7 WT binding was much smaller than the difference in fluorescence between $Im7_I$ and $Im7_N$, thus indicating that only a minor proportion of Im7 WT is unfolded to $Im7_I$ upon binding to Spy (**Supplementary Fig. 2b**). Because the binding affinity of Spy for the $Im7_I$ mimic was approximately six-fold higher than the affinity of Spy for Im7 WT (**Fig. 2b**,**c**), Spy should shift the equilibrium of $Im7_N$ toward $Im7_I$. Consistently with the known differences in K_d, the amplitude of the postburst-phase exponential of Spy–Im7 WT binding represented only 3% of the total fluorescence-intensity difference between $Im7_N$ and $Im7_I$ (**Supplementary Fig. 2b**). Most notably, the k_{obs} for the postburst-phase step did not decrease to 0 s^{-1} at high Spy concentrations (**Fig. 3c**). This observation suggests that Im7 actually folds and unfolds while it is bound to Spy (**Supplementary Fig. 3**). In summary, our kinetic data suggest that Spy is capable of binding to $Im7_U$, $Im7_I$ and $Im7_N$—three substantially different conformations[21–24]—and is able to promote folding and/or unfolding of the intermediate and native conformers in the bound state.

Im7 folds while it is bound to Spy

To further examine whether Im7 can fold or unfold while it is bound to Spy, we next directly investigated how Spy affects Im7 folding (**Fig. 1**). We denatured Im7 WT in 8 M urea and monitored folding in a stopped-flow fluorimeter by diluting the unfolded Im7 WT into buffer containing various concentrations of Spy (**Fig. 4b**). Folding of Im7 slowed as the concentration of Spy increased. Whereas the fluorescence decrease for Im7 folding in the absence of Spy (reflecting the I-to-N transition) could be fitted to a single exponential, the fluorescence decrease for Im7 folding in the presence of an equimolar concentration (5 μM) of Spy required two exponentials to achieve a

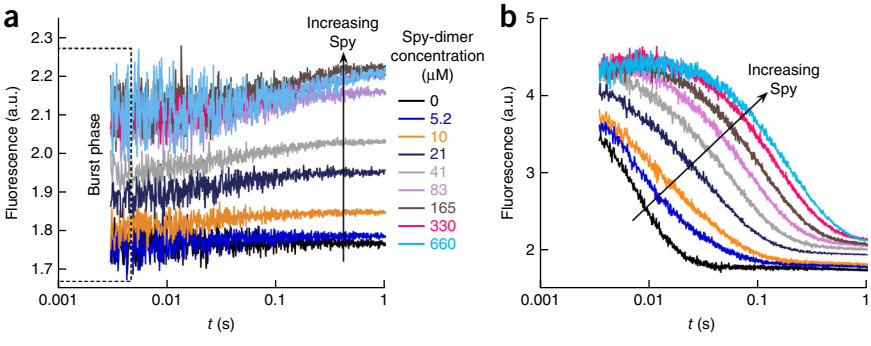

Figure 4 Stopped-flow fluorescence traces of Spy–Im7 WT binding and of Im7 folding in the presence of Spy. (**a**) Traces for Spy binding to Im7 WT under native conditions. The fluorescence of the first data point for each trace is higher than the fluorescence of Im7 WT alone (black trace) and reaches a saturating fluorescence at high Spy concentrations. This burst phase is consistent with Spy binding $Im7_N$ within the dead time of the instrument. (**b**) Traces for folding of Im7 WT in the presence of different Spy concentrations. Im7 folding slows as the concentration of Spy is increased. An increase in fluorescence in the first 20 ms occurs in the traces at the highest Spy concentrations; this phase represents the conversion of $Im7_U$ to $Im7_I$ during Im7 folding that is slowed by Spy. The Spy dimer concentrations used in **a** and **b** are identical for each color. The *y* axes are different in **a** and **b**, but the final fluorescence at 1 s is the same in both experiments, thus suggesting that the same equilibrium is reached.

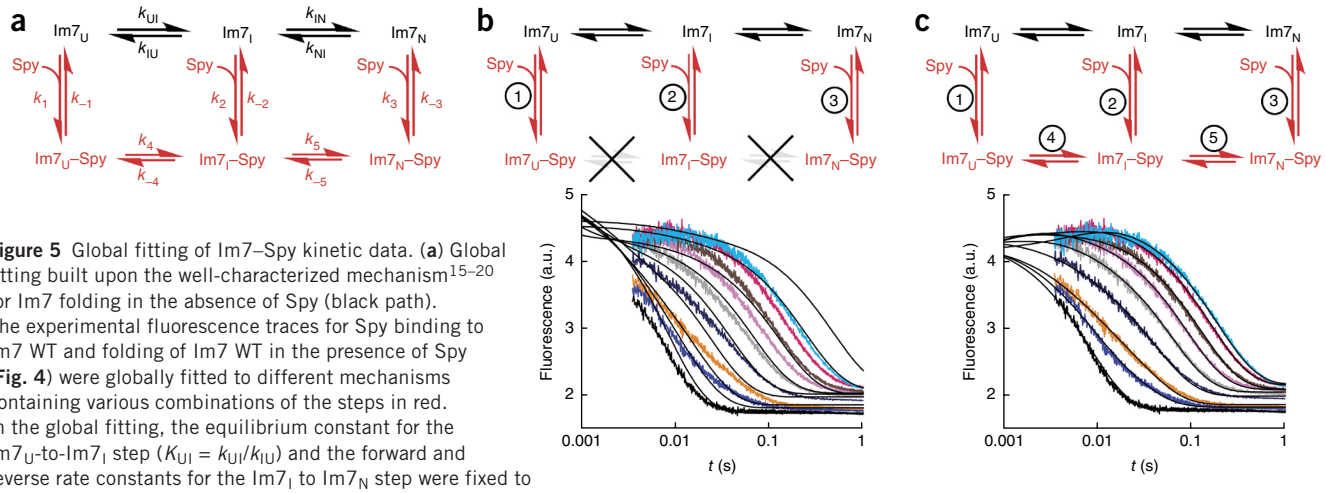

Figure 5 Global fitting of Im7–Spy kinetic data. (**a**) Global fitting built upon the well-characterized mechanism[15–20] for Im7 folding in the absence of Spy (black path). The experimental fluorescence traces for Spy binding to Im7 WT and folding of Im7 WT in the presence of Spy (**Fig. 4**) were globally fitted to different mechanisms containing various combinations of the steps in red. In the global fitting, the equilibrium constant for the $Im7_U$-to-$Im7_I$ step ($K_{UI} = k_{UI}/k_{IU}$) and the forward and reverse rate constants for the $Im7_I$ to $Im7_N$ step were fixed to the values determined from the urea dependence of Im7 folding in the absence of Spy (**Supplementary Fig. 5**). (**b**,**c**) Attempted global fitting to the mechanism that omits (**b**) or allows (**c**) the folding of Im7 while it is bound to Spy. For clarity, only the traces for Im7 folding in the presence of Spy are shown. The black lines in the plots are the best fit to the data. The mechanism that completely omits folding of Im7 while it is bound to Spy (**b**) fails to fit the data, whereas the mechanism that allows folding of Im7 while it is bound (**c**) can successfully fit the data. Global fitting to additional mechanisms and the best fit for the Spy–Im7 WT binding data are shown in **Supplementary Figure 6**.

reasonable fit, and at ≥160 μM Spy, an additional third phase, which increased in fluorescence, appeared at the beginning of the traces (**Supplementary Fig. 4a–f**). The k_{obs} values for all of the phases decreased with increasing concentrations of Spy but did not go to zero (**Supplementary Fig. 4g–i**). This combination of results indicates that Im7 is able to fold in the presence of Spy, even at concentrations of the chaperone well above the K_d for the interaction, i.e., when essentially all of the Im7 is chaperone bound. The final fluorescence intensities obtained in these refolding experiments at various concentrations of Spy were indistinguishable from those when Spy was added to native Im7, thus suggesting that both experiments reached the same thermodynamic end point.

Using all of the kinetic measurements, we next determined the complete protein-folding mechanism of Im7 in the presence of Spy by globally fitting the fluorescence transients for the two experiments (the folding of Im7 WT in the presence of Spy and the binding of Spy to Im7 WT) to various possible models in KinTek Explorer[27]. The same kinetic mechanism should govern both experiments, because the only difference between the two was the initial folding status of Im7. Convergence during global fitting of the raw fluorescence traces is rigorous in that it requires that the model adequately explain both the changes in k_{obs} and the kinetic amplitudes as a function of Spy concentration for all transients. The kinetic mechanisms tested were built upon the well-characterized three-state on-pathway mechanism for Im7 folding in the absence of Spy[15–20]; we then increased the complexity of the tested models in a stepwise fashion until we identified a mechanism that could adequately describe all of the data (**Fig. 5a**). To help constrain the global fitting, we fixed the equilibrium constant for the conversion of unbound $Im7_U$ to unbound $Im7_I$ (K_{UI}) and the forward and reverse rate constants (k_{IN} and k_{NI}, respectively) for the conversion of unbound $Im7_I$ to unbound $Im7_N$ to the known values obtained from the urea dependence for Im7 folding and unfolding (**Supplementary Fig. 5**).

Strikingly, the mechanism that omits folding of Im7 while it is bound to Spy (**Fig. 5b**) could not fit the experimental traces. This is because, in this mechanism, Im7 must first be released from Spy before it can continue folding, thus making Spy a competitive inhibitor of Im7 folding; as a result, the mechanism in **Figure 5b** predicts that k_{obs} for all phases should reach 0 s^{-1} at high Spy concentrations, in marked contrast with our experimental observations. This result shows that chaperones do not necessarily need to release bound substrates from their surface in order for substrate folding to occur, as has been posited to be the case for several ATP-dependent chaperones[1].

We achieved a good fit only when we globally fitted the data to a kinetic mechanism that allows both folding steps 4 and 5 (i.e., complete folding of Im7 while it is bound to Spy) (**Fig. 5c**); thus, this is the simplest kinetic mechanism that can explain all of the experimental data. None of the 11 other mechanisms that we tested resulted in a good fit (**Supplementary Fig. 6**). As a final validation of the mechanism in **Figure 5c**, we attempted to fit simultaneously the three data sets obtained to a common kinetic mechanism; i.e., we globally fitted the raw fluorescence transients for the urea dependence of Im7 folding and unfolding, the transients for Im7 folding in the presence of Spy and the kinetic traces obtained during the binding of Spy to Im7 WT to the mechanism shown in **Figure 5c** (**Supplementary Fig. 7**). Doing so further constrained the model by simultaneously enforcing the same fluorescence scaling factors and rate constants upon all of the raw data for all of the experiments used in the analysis. If such a fit can be achieved, this represents a rigorous test of the kinetic model[27–30]. We achieved an excellent fit (**Table 1** and **Supplementary Fig. 7**); the K_d values for Spy binding to $Im7_U$, $Im7_I$ and $Im7_N$ obtained from the global fit were similar to the experimental values obtained by ITC for Spy binding to the $Im7_U$ mimic, the $Im7_I$ mimic and Im7 WT (**Supplementary Table 1**). In addition, the relative fluorescence intensities generated from the fit for the different species in the kinetic mechanism were similar to the relative fluorescence intensities of the $Im7_U$ mimic, the $Im7_I$ mimic and Im7 WT, and their complexes with Spy, thus further validating the mechanism (**Supplementary Table 1**). The global analysis also satisfied the thermodynamic cycles of the mechanism in **Figure 5c** by maintaining a zero net free-energy change around each cycle.

DISCUSSION

Our data indicate that Spy can bind to multiple conformers of Im7 and that Spy actually allows Im7 to fold while it is bound to the chaperone surface. The forward rate constants for folding of Spy-bound Im7 obtained by global analysis were 30–40 times lower than the

Table 1 Rate constants obtained from global fit of kinetic data to mechanism (Fig. 5c) that allows complete folding of Im7 while it is bound to Spy

	Rate constant[a] (s^{-1} or M^{-1} s^{-1})
k_{UI}	1,610 ± 210
k_{IU}	1,940 ± 180
k_{IN}	286 ± 23
k_{NI}	0.99 ± 0.01
k_1	$1.4 \pm 0.2 \times 10^7$
k_{-1}	65 ± 14
k_2	$1.7 \pm 0.2 \times 10^7$
k_{-2}	79 ± 17
k_3	$3.3 \pm 0.4 \times 10^7$
k_{-3}	1,000[b]
k_4	51 ± 12
k_{-4}	62 ± 11
k_5	10.1 ± 2.1
k_{-5}	0.23 ± 0.01

[a]Values in 0.7 M urea. Determined by global analysis of all data (**Supplementary Fig. 7**). Values reported are the mean ± s.e.m. of the fit. [b]Fixed at 1,000 s^{-1}.

corresponding rate constants for Im7 folding in solution (**Table 1**), thus indicating that there is a kinetic penalty associated with folding of Im7 while it is bound to Spy. Nonetheless, the folding rate of Im7 while it is bound to Spy still occurs on a subsecond timescale, much faster than transcription or translation and thus fast enough to be physiologically relevant. This ability of Spy to allow folding of bound substrates is probably an essential component of its function *in vivo*—if folding of Spy-bound substrates were not possible, protein folding would be inhibited at the ~2 mM concentration of Spy that is present *in vivo* during stress. Previously, barnase has been shown to fold while it is bound to the cavity of the GroEL ring in the absence of ATP and GroES, at a slower rate than it folds when it is free in solution[31,32]. More recently, a mutant of the model protein substrate Fyn SH3 domain ($SH3^{Mut}$) has been shown by NMR to fold and unfold into a partially folded intermediate state while it is bound within the double-ring structure of GroEL, in the absence of ATP and GroES; this process occurs at rates substantially faster than the rates of $SH3^{Mut}$ folding and unfolding when it is free in solution[33]. GroEL can therefore accelerate or decelerate substrate folding, depending on the protein, whereas Spy, to date, has been shown to only decelerate the folding of Im7. The folding rate constant of $SH3^{Mut}$ is approximately three times higher while $SH3^{Mut}$ is bound to GroEL, whereas the unfolding rate constant is ~500 times higher in this bound state, thus leading to a dramatic stabilization of the intermediate state over the native state of $SH3^{Mut}$ and contributing to GroEL's intrinsic unfoldase activity[33]. In contrast, Spy binds $Im7_I$ and $Im7_U$ with an affinity only approximately six-fold higher than that of $Im7_N$, and therefore it does not substantially destabilize the native state of bound Im7. In contrast to Spy, which has to function *in vivo* in the absence of an energy source and the assistance of cochaperones, GroEL and many other chaperone systems use ATP and cochaperones (such as GroES) to control substrate binding and release[1,6,34–36]. However, that both Spy and GroEL allow protein folding while they are bound to substrate raises the intriguing possibility that folding while the substrate is flexibly bound may represent the underlying basis for the action of multiple chaperones. The evolutionary addition of ATP and cochaperone dependencies would then serve as enhancements to help control chaperone action. It has previously been thought that only ATP-dependent 'foldase' chaperones can actively facilitate protein folding. The ATP-independent 'holdase' chaperones have been thought to play a more passive role, holding onto aggregation-sensitive folding intermediates and thereby inhibiting aggregation until they can transfer these intermediates to foldases, which then actively fold the substrate proteins. Our finding that proteins can fold while they are loosely bound to the surface of Spy suggests that ATP-independent chaperones may have a more active role in protein folding than has been surmised previously.

In light of our findings, we propose the following model for how Spy operates *in vivo* (**Fig. 6**). Upon chemical stress such as exposure to butanol or tannins, Spy production is upregulated, thus rapidly transforming the periplasmic concentration from near zero under nonstress conditions to ~2 mM in the presence of stress[10,12,13]. At these concentrations, Spy rapidly (on a submillisecond timescale) associates most tightly with proteins that are at least partially or transiently unfolded by the stressors. At high Spy concentrations, the majority of these unfolded proteins are bound to Spy, thus preventing their aggregation. Once the stress is removed, refolding of the substrate protein becomes energetically more favorable. We have shown that Spy allows Im7 to fold into its native state while it remains bound to the chaperone. This mechanism minimizes the concentration of unbound, aggregation-sensitive protein-folding intermediates while still allowing the timely folding of substrates to their aggregation-insensitive native state before release. We expect that the dilution of Spy through degradation or cell growth after a return to nonstress conditions gradually lowers the Spy concentration, thus leading to the release of substrate proteins in their native state by mass action (**Supplementary Movie 1**). Spy thus provides proteins with a sanctuary from stress that allows refolding while preventing aggregation.

In summary, we provided evidence that the ATP-independent chaperone Spy rapidly associates with many different conformers (U, I and N) of its substrate proteins, at least as exemplified by Im7, the protein

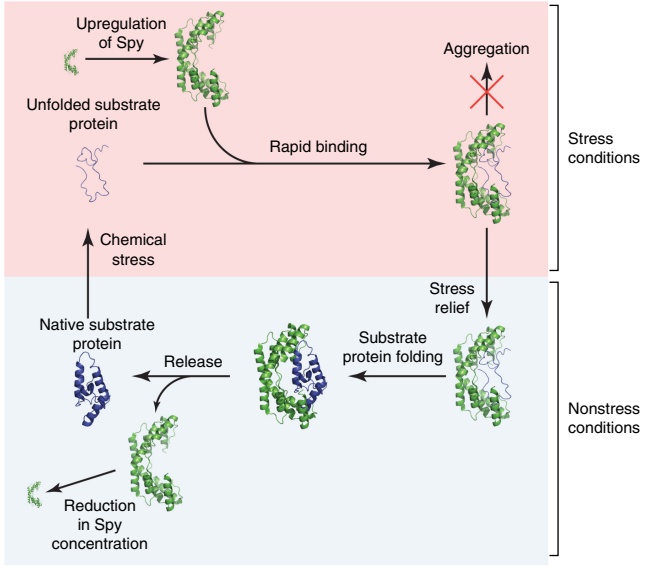

Figure 6 Proposed mechanism for how Spy inhibits aggregation and assists in protein folding *in vivo*. Clockwise from the bottom left (native substrate protein), exposure to chemical stress (denoted by the pink box) causes proteins in the periplasm of *E. coli* to unfold. The stress induces the production of Spy, which rapidly associates with its substrate proteins, thereby preventing their aggregation. Once the stress is removed (denoted by the light blue box), dilution of Spy through cell growth or degradation lowers the Spy concentration, thus allowing the native substrate protein to be released.

for which Spy was first discovered as a chaperone[10]. Spy allows folding while its substrate is bound, thereby preventing the irreversible aggregation of proteins that may otherwise detrimentally affect the cell. By binding to all three populated states with similar affinities, Spy allows Im7 to fold in the bound state without substantially altering its folding energy landscape. The surface of Spy therefore is tuned to accommodate not only multiple substrate proteins[10,14] but also drastically different conformations of the same protein. Spy binds substrates with a relatively modest (micromolar) affinity, which is probably necessary for the chaperone to promiscuously bind multiple substrates and multiple folding conformations of the same protein. This finding is consistent with a theoretical model for how chaperones work in which loose binding allows substrate folding[37]. We speculate that the principle of binding multiple conformations and allowing protein folding while the substrate is loosely bound may represent the primordial basis of chaperone action.

METHODS

Methods and any associated references are available in the online version of the paper.

Note: Any Supplementary Information and Source Data files are available in the online version of the paper.

ACKNOWLEDGMENTS

We thank S. Horowitz for critical reading of the manuscript. This work was funded by a Boehringer Ingelheim Fonds fellowship (P.K.) and US National Institutes of Health grant GM102829 (J.C.A.B. and S.E.R.), which also funded J.R.H. J.C.A.B. is supported as a Howard Hughes Investigator.

AUTHOR CONTRIBUTIONS

F.S., P.K. and J.R.H. performed the experiments. All authors analyzed the data. F.S., S.E.R. and J.C.A.B. designed the study. F.S. wrote the manuscript, with contributions from all other authors.

COMPETING FINANCIAL INTERESTS

The authors declare no competing financial interests.

1. Hartl, F.U., Bracher, A. & Hayer-Hartl, M. Molecular chaperones in protein folding and proteostasis. *Nature* **475**, 324–332 (2011).
2. Buchner, J. Hsp90 & Co.: a holding for folding. *Trends Biochem. Sci.* **24**, 136–141 (1999).
3. Zuiderweg, E.R.P. *et al.* Allostery in the Hsp70 chaperone proteins. *Top. Curr. Chem.* **328**, 99–153 (2013).
4. Priya, S., Sharma, S.K. & Goloubinoff, P. Molecular chaperones as enzymes that catalytically unfold misfolded polypeptides. *FEBS Lett.* **587**, 1981–1987 (2013).
5. Saibil, H. Chaperone machines for protein folding, unfolding and disaggregation. *Nat. Rev. Mol. Cell Biol.* **14**, 630–642 (2013).
6. Horwich, A.L. & Fenton, W.A. Chaperonin-mediated protein folding: using a central cavity to kinetically assist polypeptide chain folding. *Q. Rev. Biophys.* **42**, 83–116 (2009).
7. Jakob, U., Gaestel, M., Engel, K. & Buchner, J. Small heat shock proteins are molecular chaperones. *J. Biol. Chem.* **268**, 1517–1520 (1993).
8. Tapley, T.L., Franzmann, T.M., Chakraborty, S., Jakob, U. & Bardwell, J.C.A. Protein refolding by pH-triggered chaperone binding and release. *Proc. Natl. Acad. Sci. USA* **107**, 1071–1076 (2010).
9. Hoffmann, A., Bukau, B. & Kramer, G. Structure and function of the molecular chaperone Trigger Factor. *Biochim. Biophys. Acta* **1803**, 650–661 (2010).
10. Quan, S. *et al.* Genetic selection designed to stabilize proteins uncovers a chaperone called Spy. *Nat. Struct. Mol. Biol.* **18**, 262–269 (2011).
11. Dahl, J.-U. *et al.* HdeB functions as an acid-protective chaperone in bacteria. *J. Biol. Chem.* **290**, 65–75 (2015).
12. Brynildsen, M.P. & Liao, J.C. An integrated network approach identifies the isobutanol response network of *Escherichia coli*. *Mol. Syst. Biol.* **5**, 277 (2009).
13. Rutherford, B.J. *et al.* Functional genomic study of exogenous n-butanol stress in *Escherichia coli*. *Appl. Environ. Microbiol.* **76**, 1935–1945 (2010).
14. Quan, S. *et al.* Super Spy variants implicate flexibility in chaperone action. *eLife* **3**, e01584 (2014).
15. Ferguson, N., Capaldi, A.P., James, R., Kleanthous, C. & Radford, S.E. Rapid folding with and without populated intermediates in the homologous four-helix proteins Im7 and Im9. *J. Mol. Biol.* **286**, 1597–1608 (1999).
16. Capaldi, A.P., Shastry, M.C.R., Kleanthous, C., Roder, H. & Radford, S.E. Ultrarapid mixing experiments reveal that Im7 folds via an on-pathway intermediate. *Nat. Struct. Biol.* **8**, 68–72 (2001).
17. Capaldi, A.P., Kleanthous, C. & Radford, S.E. Im7 folding mechanism: misfolding on a path to the native state. *Nat. Struct. Biol.* **9**, 209–216 (2002).
18. Friel, C.T., Capaldi, A.P. & Radford, S.E. Structural analysis of the rate-limiting transition states in the folding of Im7 and Im9: similarities and differences in the folding of homologous proteins. *J. Mol. Biol.* **326**, 293–305 (2003).
19. Knowling, S.E., Figueiredo, A.M., Whittaker, S.B.M., Moore, G.R. & Radford, S.E. Amino acid insertion reveals a necessary three-helical intermediate in the folding pathway of the colicin E7 immunity protein Im7. *J. Mol. Biol.* **392**, 1074–1086 (2009).
20. Friel, C.T., Smith, D.A., Vendruscolo, M., Gsponer, J. & Radford, S.E. The mechanism of folding of Im7 reveals competition between functional and kinetic evolutionary constraints. *Nat. Struct. Mol. Biol.* **16**, 318–324 (2009).
21. Spence, G.R., Capaldi, A.P. & Radford, S.E. Trapping the on-pathway folding intermediate of Im7 at equilibrium. *J. Mol. Biol.* **341**, 215–226 (2004).
22. Gsponer, J. *et al.* Determination of an ensemble of structures representing the intermediate state of the bacterial immunity protein Im7. *Proc. Natl. Acad. Sci. USA* **103**, 99–104 (2006).
23. Whittaker, S.B.M., Spence, G.R., Günter Grossmann, J., Radford, S.E. & Moore, G.R. NMR analysis of the conformational properties of the trapped on-pathway folding intermediate of the bacterial immunity protein Im7. *J. Mol. Biol.* **366**, 1001–1015 (2007).
24. Pashley, C.L. *et al.* Conformational properties of the unfolded state of Im7 in nondenaturing conditions. *J. Mol. Biol.* **416**, 300–318 (2012).
25. Vogt, A.D. & Di Cera, E. Conformational selection or induced fit? A critical appraisal of the kinetic mechanism. *Biochemistry* **51**, 5894–5902 (2012).
26. Gianni, S., Dogan, J. & Jemth, P. Distinguishing induced fit from conformational selection. *Biophys. Chem.* **189**, 33–39 (2014).
27. Johnson, K.A., Simpson, Z.B. & Blom, T. Global kinetic explorer: a new computer program for dynamic simulation and fitting of kinetic data. *Anal. Biochem.* **387**, 20–29 (2009).
28. Jahn, T.R., Parker, M.J., Homans, S.W. & Radford, S.E. Amyloid formation under physiological conditions proceeds via a native-like folding intermediate. *Nat. Struct. Mol. Biol.* **13**, 195–201 (2006).
29. Huddleston, J.P., Schroeder, G.K., Johnson, K.A. & Whitman, C.P. A pre-steady state kinetic analysis of the αY60W mutant of trans-3-chloroacrylic acid dehalogenase: implications for the mechanism of the wild-type enzyme. *Biochemistry* **51**, 9420–9435 (2012).
30. Schroeder, G.K. *et al.* Reaction of cis-3-chloroacrylic acid dehalogenase with an allene substrate, 2,3-butadienoate: hydration via an enamine. *J. Am. Chem. Soc.* **134**, 293–304 (2012).
31. Gray, T.E. & Fersht, A.R. Refolding of barnase in the presence of GroE. *J. Mol. Biol.* **232**, 1197–1207 (1993).
32. Corrales, F.J. & Fersht, A.R. The folding of GroEL-bound barnase as a model for chaperonin-mediated protein folding. *Proc. Natl. Acad. Sci. USA* **92**, 5326–5330 (1995).
33. Libich, D.S., Tugarinov, V. & Clore, G.M. Intrinsic unfoldase/foldase activity of the chaperonin GroEL directly demonstrated using multinuclear relaxation-based NMR. *Proc. Natl. Acad. Sci. USA* **112**, 8817–8823 (2015).
34. Fink, A.L. Chaperone-mediated protein folding. *Physiol. Rev.* **79**, 425–449 (1999).
35. Young, J.C. & Hartl, F.U. Polypeptide release by Hsp90 involves ATP hydrolysis and is enhanced by the co-chaperone p23. *EMBO J.* **19**, 5930–5940 (2000).
36. Mayer, M.P. & Bukau, B. Hsp70 chaperones: cellular functions and molecular mechanism. *Cell. Mol. Life Sci.* **62**, 670–684 (2005).
37. Jewett, A.I. & Shea, J.E. Folding on the chaperone: yield enhancement through loose binding. *J. Mol. Biol.* **363**, 945–957 (2006).

ONLINE METHODS

Protein expression and purification. WT Spy was purified as described previously[10], with the exception that Ni-HisTrap columns (GE Healthcare) were used in place of the Ni-NTA beads and mini chromatography column. After purification on the Ni-HisTrap column, WT Spy was treated with ULP1 to cleave the SUMO tag during dialysis into 40 mM Tris HCl, pH 8, and 300 mM NaCl. After dialysis, Spy was passed over the HisTrap column to remove the cleaved SUMO tag. The flow through was exchanged into 20 mM Tris HCl, pH 8, by five cycles of concentration and dilution in a 10-kDa-cutoff Amicon centrifugal filter unit. Spy was then passed over a HiTrap Q column. Spy has an isoelectric point of 9.5 and therefore was collected in the flow through. The flow through containing Spy was buffer-exchanged into 50 mM sodium phosphate buffer, pH 6.5, loaded onto a HiTrap SP column, and eluted with an 0–1 M NaCl gradient in 50 mM sodium phosphate buffer, pH 6.5. Spy was then further purified with a HiLoad 75 gel-filtration column in 40 mM HEPES-KOH, pH 7.5, 100 mM NaCl. Fractions containing Spy were concentrated, frozen in liquid nitrogen, and stored at −80 °C. Im7 L18A L19A L37A, Im7 L53A I54A, and Im7 WT were purified with the same protocol, except that the Im7 was retained by the Q column. (The isoelectric point of Im7 is 4.5.) Im7 was eluted from the Q column with an NaCl gradient of 0–1 M. The SP-column step was not used in purifying Im7 WT or the Im7 variants.

Isothermal titration calorimetry (ITC). ITC was performed with a MicroCal iTC200 in 40 mM HEPES-KOH, pH 7.5, and 100 mM NaCl at 10 °C with Im7 in the cell and Spy in the titration syringe. 150 μM Im7 L18A L19A L37A, 50 μM Im7 L53A I54A, and 230 μM Im7 WT were titrated with 1.65 mM, 550 μM and 2.53 mM Spy dimer, respectively. 1.0-μL injections were used for the titrations with Im7 L18A L19A L37A and Im7 L53A I54A. 1.5-μL injections were used for the titration with Im7 WT. ITC thermograms were fitted to a one-site model with the Origin software provided with the instrument.

Stopped-flow fluorescence experiments. Stopped-flow experiments were performed at 10 °C in 40 mM HEPES-KOH, pH 7.5, and 100 mM NaCl with a KinTek SF-2004 or an Applied Photophysics SX18.MV stopped-flow instrument. Fluorescence of the single tryptophan of Im7 was excited at 296 nm with a 4-nm band pass, and the fluorescence emission signal was collected through a 340 ± 10 nm band-pass filter. A 1:1 mix was used for the experiments monitoring the binding of Spy to the different Im7 variants. Final Im7 concentrations were 5 μM, 0.5 μM, and 4.8 μM for Im7 L18A L19A L37A, Im7 L53A I54A, and Im7 WT, respectively. The urea dependence of Im7 folding and unfolding in the absence of Spy was determined as described previously[15,16,20]. To measure folding of Im7 in the presence of different Spy concentrations, a 1:10.5 mix was used to mix 55 μM of Im7 WT in 8 M urea with buffer containing various concentrations of Spy (0–660 μM dimer after mixing). The final concentration of Im7 WT after mixing was 4.8 μM, and the urea concentration after mixing was 0.7 M. For the experiment measuring Spy binding to Im7 WT, 0.7 M urea was also included in the buffer so that the buffer conditions were identical to the final buffer conditions in the experiments measuring Im7 folding in the presence of Spy. 10–15 traces were averaged for each data point in the experiments measuring Spy binding to the Im7 variants, and 7–10 traces were averaged for each data point in the experiments measuring Im7 folding. The tyrosine of Spy contributed some background fluorescence to the stopped-flow traces, especially at higher Spy concentrations. To remove this background fluorescence, shots of Spy diluted against buffer were collected at each Spy concentration, which were then subtracted from the traces for experiments containing Im7. Observed rate constants were obtained by fitting individual traces to sums of exponentials with KaleidaGraph (Synergy Software).

Simulations of Spy–Im7 WT binding kinetics. Simulations of the change in k_{obs} with Spy concentration for the two mechanisms in **Supplementary Figure 3** were run in Berkeley Madonna (University of California at Berkeley), which can numerically solve the differential equations describing the two kinetic schemes depicted in this figure. Simulations of experimental traces were generated by defining the kinetic scheme and initial conditions at several different Spy concentrations. The forward and reverse rate constants for the $Im7_I$-to-$Im7_N$ step used in the simulations were the values determined at 0.7 M urea from the denaturant dependence of Im7 folding in the absence of Spy (**Supplementary Fig. 5**). k_{on} and k_{off} for Spy binding to $Im7_I$ and $Im7_N$ were chosen so that the affinity of Spy for $Im7_I$ and $Im7_N$ would equal the values determined from the ITC titrations (**Fig. 2**) and so that binding of Spy to Im7 would be rapid relative to the conformational-change step. (k_{off} and the apparent k_{on} rate constants are much greater than the rate constants for the conformational change.) The folding and unfolding rate constants for Im7 bound to Spy in **Supplementary Figure 3b** were selected to maintain a zero net free energy around the thermodynamic cycle and so that the sum of the forward and reverse rate constants for the $Im7_I$-to-$Im7_N$ step in the bound state would equal 3.5 s^{-1}. 4.785 μM $Im7_N$ and 0.015 μM $Im7_I$ were used as the initial conditions (in agreement with the equilibrium constant of 319 in 0.7 M urea for the $Im7_I$-to-$Im7_N$ step, as determined by the urea dependence of Im7 folding and unfolding in the absence of Spy (**Supplementary Fig. 5**)). Traces of the slow step in the simulation were subsequently fitted in KaleidaGraph (Synergy Software) to a single exponential to obtain the observed rate constants at different Spy concentrations. The limiting rate constant of the slow step at infinite Spy concentration was determined by fitting plots of k_{obs} against Spy concentration from the simulated traces to an inverse-square hyperbola.

Global fitting of kinetic data. The stopped-flow fluorescence traces for Spy binding to Im7 WT under nondenaturing conditions and the traces for Im7 folding in the presence of different Spy concentrations were globally fitted to various kinetic mechanisms in KinTek Explorer (KinTek Corporation)[27], version 5.1.15078, which can constrain thermodynamic cycles by maintaining a zero net free energy around the cycle. This program fits kinetic data by direct numerical integration of the rate equations that define the kinetic model; fitting in KinTek Explorer involves minimizing the global χ^2 to obtain the microscopic rate constants and the fluorescence signals of the individual species of the kinetic mechanism. The mechanisms tested were built upon the known mechanism for Im7 folding[15–20], which passes through an intermediate state before reaching the native state. When initially globally fitting the Im7 folding in the presence of Spy and Spy binding to native Im7 data to different mechanisms, the k_{IN} and k_{NI} rate constants were fixed at 345 s^{-1} and 1.08 s^{-1}, respectively, and the K_{UI} equilibrium constant (k_{UI}/k_{IU}) was fixed at 0.57; these were the values in 0.7 M urea obtained from the Im7 folding/unfolding chevron plots (**Supplementary Fig. 5**). In fitting of the Spy–Im7 WT binding traces, the Im7 was allowed to equilibrate for 10 s before the addition of Spy so that the 4.8 μM Im7 could distribute between $Im7_U$, $Im7_I$, and $Im7_N$ to the concentrations dictated by the equilibrium constants generated from the fitting before the addition of Spy. 4.8 μM $Im7_U$ was used as the initial conditions in globally fitting the Im7 folding in the presence of Spy traces. The fluorescence of $Im7_I$ and the $Im7_I$–Spy complex were set equal to one another; this constraint is consistent with there being no change in fluorescence before the conformational change when Spy binds $Im7_I$ (i.e., there is no burst phase, **Supplementary Fig. 1**). Initial global fitting indicated that the association (k_{on}) and dissociation (k_{off}) rate constants for Spy binding $Im7_N$ were poorly constrained by the data because Spy binding to $Im7_N$ occurred within the dead time in the Spy–Im7 WT binding experiment. Accordingly, k_{off} for the Spy-$Im7_N$ binding step was fixed at 1,000 s^{-1} (a reasonable lower limit given the dead time) to allow the program to simply fit the K_d for this step. During the process of global fitting, individual traces were scaled with a correction factor (<4%) to correct for slight fluctuations in lamp intensity between traces. The mechanism depicted in **Figure 5c**, which includes steps for Spy binding to $Im7_U$, $Im7_I$, and $Im7_N$ and allows for the complete folding of Im7 while it is bound to Spy, was the simplest model able to satisfactorily describe the data on the basis of the goodness of fit (χ^2) and visual inspection of the fit. The fluorescence traces for Im7 folding and unfolding at different urea concentrations were fitted on the basis of the assumption that a rate constant varies with urea concentration according to the expression $k_{xy} = k_{xy}^{H_2O} e^{(m_{xy}/RT)[Urea]}$ where k_{xy} is the rate constant for the formation of y from x, $k_{xy}^{H_2O}$ is the rate constant in 0 M urea, and m_{xy} defines the urea dependence for this step[15]. It was also assumed that the fluorescence of $Im7_U$, $Im7_I$, and $Im7_N$ changed linearly with urea concentration. From the simultaneous fitting of all of the fluorescence traces, the fluorescence of $Im7_U$, $Im7_I$, and $Im7_N$ was 0.725 + 0.055[urea], 1.070 + 0.067[urea], and 0.335 + 0.041[urea], respectively. The rate constants reported in **Table 1** are rounded to two or three significant figures.